*Technology and Science for the Ships of the Future*
*V. Crupi and V. Bucci (Eds.)*

*doi:10.3233/PMST250124*

# Characterization of Hybrid-Dissimilar Joints Using Non-Destructive Thermographic Techniques

Francesca DI CAROLO[a,1], Rosa DE FINIS[b], Davide PALUMBO[a], Ester D'ACCARDI[a], Gabriella EPASTO[c] and Umberto GALIETTI[a].
[a] *Poltechnic University of Bari, Via Edoardo Orabona, 4, 70126 Bari, BA, Italy*
[b] *University of Salento, Piazza Tancredi, n7, 73100 Lecce, LE, Italy*
[c] *University of Messina, Contrada Di Dio - Vill. Sant'Agata, 98166, Messina, ME, Italy*

ORCiD ID: Francesca Di Carolo: https://orcid.org/0000-0001-5222-0564

**Abstract.** In recent years, new manufacturing processes and joint techniques have been developed to reduce weight while improving sustainability and circularity in the design of components and structures. In this context, monitoring structures using non-destructive techniques can provide useful information about the presence of defects that can compromise the strength of the material and lead to unexpected early failure. Detecting, quantifying, and then repairing components can extend their life, increasing sustainability. The aim of this work is the non-destructive characterization by means of thermographic techniques of hybrid dissimilar materials made of a layered structure in which the bulk material (additive manufactured AlSi10Mg) is coated with carbon fibre skins. In particular, the presence of detachments between the bulk and coating has been investigated on several specimens classified according to the 3D building direction of the bulk material: 0°, 45°, 90°. Several tests were carried out adopting lock-in and step thermography using two halogen lamps with a total power of 1300 W. Data were analysed with several algorithms and a quantitative evaluation of the damaged area was performed. Moreover, the Thermoelastic Stress Analysis (TSA) has been used as an NDT technique for assessing the damaged area before tensile and bending tests. Finally, possible correlations between mechanical properties and damaged areas have been investigated by using statistical tools.

**Keywords.** Hybrid-Dissimilar Joints, Non-Destructive Testing, IR Thermography, AM, Thermoelastic Stress Analysis

## 1. Introduction

A significant challenge in naval architecture lies in creating components that not only meet stringent design specifications and deliver optimal structural performance but are also as lightweight and compact as possible. Modern design must also conscientiously address the environmental consequences of its choices. These somewhat conflicting demands can be tackled from two angles. Firstly, by developing innovative materials that optimize both the strength-to-weight ratio and the balance between structural integrity

[1] Corresponding Author: Francesca Di Carolo, francesca.dicarolo@poliba.it

and environmental impact. Secondly, by implementing targeted non-destructive testing to identify potential defects [1,2] that could compromise mechanical strength and lead to premature component failure, in fact detecting, quantifying, and then repairing components can extend their life, increasing sustainability. In this field, there's a strong focus on components that can exploit the complementary strengths of different materials by joining them with innovative methods. These are known as hybrid or dissimilar joints, and they are widely used in various types of marine vessels. Their popularity is due to their capacity to deliver optimal performance across several areas simultaneously: they offer robust mechanical strength while minimizing weight and size, which in turn enhances environmental sustainability. There are several ways to create these dissimilar or hybrid joints, including Friction Stir Welding, Explosion Welding, and adhesive bonding, to name just a few [3,4]. The innovative nature of these technologies often means there's limited understanding of the components' mechanical characteristics. Consequently, there can be some reluctance to adopt them in place of more traditional solutions which, though less sustainable and efficient, are perceived as more reliable. This challenge can be addressed by developing non-destructive testing (NDT) procedures. These procedures serve a dual purpose: firstly, to mechanically characterize the joints, and secondly, to enable structural health monitoring of the components, thereby increasing their reliability [5-7]. Compared to other full-field NDT methods like X-ray and tomography, thermographic techniques can be an optimal solution, offering non-contact, full-field capabilities, time-saving procedures, low energy consumption, and no consumables [8-13].

In this work the use of thermographic techniques for non-destructively evaluating hybrid dissimilar materials was explored. The materials consist of an additively manufactured (AM) AlSi10Mg core, which is then coated with carbon fiber skins. The primary investigation was focused on identifying detachments between this core and its coating across various samples, which were grouped based on the 3D printing orientation (0°, 45°, 90°) of the AlSi10Mg. Lock-In thermography (LT) was employed, using two halogen lamps providing a total of 1300W for thermal excitation. The collected data were processed with multiple algorithms to quantify the extent of any damage. Additionally, Thermoelastic Stress Analysis (TSA) served as a non-destructive tool to evaluate damage before the specimens underwent tensile and bending tests [14-17]. Furthermore, potential relationships between the detected damaged areas and the materials' mechanical properties were observed.

## 2. Thermographic NDTs

In this section the Thermographic NDT techniques employed to characterize the samples are described.

Active thermography is a dynamic analysis technique used for material evaluation. It involves stimulating the material with external energy sources to analyze its thermal response. Typically, pulsed flash lamps or lasers, periodic laser signals, and halogen lamps are used. Mechanical excitation, through the application of periodic dynamic loads that exploit the thermoelastic effect, can also be employed [8-11].

Active thermographic techniques can be classified based on the specific method employed, which relates to how the thermal stimulation is delivered, and by the type of excitation source. In particular, two techniques were employed in this work: Lock-in Thermography and Thermoelastic Stress Analysis (TSA) [16].

### *2.1. Lock-In Thermography*

Lock-in Thermography (LT) is an active thermal inspection technique that analyzes the material's response to periodic heating. A heat source is modulated at a specific frequency, and the resulting periodic temperature changes on the material's surface are monitored. This data is then processed, often pixel by pixel, to create two main types of images: amplitude and phase [9-11].

The phase image, which shows the time lag of the temperature response relative to the heat stimulus, is particularly useful for detecting sub-surface features, defects, or variations in thermal properties like thermal diffusivity, as these affect the thermal wave's propagation time. The amplitude image, representing the magnitude of the temperature oscillation, provides information about the intensity of heating, surface characteristics, or variations in thermal effusivity.

The propagation of these thermal waves can be mathematically modeled for a semi-infinite body in adiabatic conditions as [9]:

$$T(z,t) = T_0 exp\left(-\frac{z}{\mu}\right)\cos\left(\frac{2\pi z}{\lambda} - \omega t\right) \quad (1)$$

Thermoelastic Stress Analysis (TSA) exploits the principle that solids change temperature when stressed (cooling under tension, heating under compression), allowing surface stress evaluation through dynamic thermal monitoring [14-17].

For homogeneous, isotropic materials under adiabatic conditions (typically achieved with sinusoidal loading), the core relationship between peak-to-peak temperature change ΔT and the peak-to-peak change in the sum of principal stresses ($\Delta\sigma_{11} + \Delta\sigma_{22}$) is [16]:

$$\Delta T = -T_0 K_0(\Delta\sigma_{11} + \Delta\sigma_{22}) \quad (2)$$

The factor $K_0$ incorporates the material's thermoelastic constant, and it is defined as:

$$K_0 = \frac{\alpha}{\rho C_p} \quad (3)$$

The induced temperature variations are captured as a sinusoidal signal:

$$T(t) = T_0 + \Delta T \sin(\omega t + \varphi)) \quad (4)$$

This requires high-sensitivity (often cooled) thermal cameras. Extracting the signal amplitude $\Delta T$ and phase $\varphi$ from data, which typically has a low signal-to-noise ratio, necessitates careful processing, often using algorithms similar to those in Lock-in Thermography.

As an NDT tool, TSA is valuable for applications like monitoring adhesive bond integrity and tracking damage progression during fatigue tests by analyzing thermal signal changes.

## 3. NDT experimental campaign

Thermographic NDTs were conducted on sandwich specimens produced using AM techniques, and AlSi10Mg as the base material.

The AlSi10Mg core is coated with carbon fiber skins through an adhesive bonding.

The carbon coating is composed of two layers, each of which has carbon fibers arranged in two directions, in order to make the material as isotropic as possible. The first bidirectional layer has an orientation of 90°/-90°, while the second has an orientation of 45°/-45°.

The study involved twelve specimens (Figure 1), which were of two types. The first type included dog-bone samples for tensile tests, with a useful section measuring 70 x 12.5 x 3 mm. The second type consisted of rectangular samples for bending tests, with dimensions of 100 x 12.7 x 3 mm. Duplicates of each sample type were prepared using three different printing directions: 0°, 45°, and 90°.

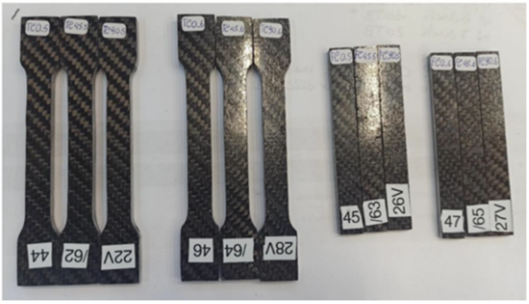


**Figure 1.** AlSi10Mg samples

For LT, a FLIR A655sc microbolometer thermal camera with an acquisition frequency of 25 Hz was used. The IR camera was placed at a distance of 240 mm for the tensile specimens (tested three at a time) and at a distance of 395 mm for the flexural specimens (tested all six together).

LT was performed using two halogen lamps, each with a power of 650 W (1.3 kW in total), were used as excitation source and the tests were performed with three different excitation (heating) periods, equal to 5, 20 and 35 s. In Figure 2 (a) the test setup is shown.

TSA tests were performed only on the six dog-bone samples.

For TSA tests a cooled FLIR X6540sc thermal imaging camera (Figure 2) with an acquisition frequency of 190 Hz was used. The tensile testing machine was equipped with a 50 kN load cell. The specimens were gripped with a jaw pressure of 3.5 MPa and TSA tests were performed at 3, 7 and 11 Hz for each specimen. Figure 2 (b) shows the experimental set up.


(a)

(b)

**Figure 2.** Experimental setup for (a) LT tests and (b) TSA tests.

The processing of the thermographic sequences and their related analysis was carried out using the IRTA 2 software.

## 4. Mechanical Testing

The same specimens tested with NDT thermographic techniques were then subjected to static mechanical characterization tests, specifically tensile tests for the dog-bone specimens and three-point bending tests for the rectangular specimens. The loading machine used is a servo-hydraulic machine with a 50 kN load cell, and the two configurations are shown in Figure 3.

Both test modes were carried out in displacement control, imposing a speed of 2 mm/min for the lower crosshead: downwards for the tensile tests and upwards for the bending tests.

The displacement field during the tensile tests was also measured with a clip-on extensometer (gauge length 25 mm).

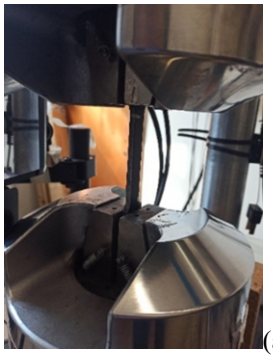
(a)

(b)

**Figure 3.** Experimental setup for (a) tensile and (b) bending tests.

## 5. Results

In this section only the main results are presented.

These tests focus solely on the qualitative evaluation of damaged areas. They are not intended to provide an accurate evaluation of the extent of the defect. Their only purpose

is to show areas on the specimens where heat spreads differently, which suggests that debonding has occurred.

### *5.1. LT Results*

The results from the thermographic tests are shown as signal phase maps. We are only showing the results from the test period that gave us the best signal-to-noise ratio.

Figure 4 a and Figure 5 display the phase maps corresponding to a 5s period for the tensile and bending specimens, respectively. Figure 4 presents some indications of anomalies especially on specimens T1 45° side A, B1 45° side A and B2 45° side A.

### *5.2. TSA Results*

The results of the TSA analyses are reported only for the tensile specimen T5 45 side A presenting an anomaly (possibly a delamination) in agreement with the LT results. In particular, the signal amplitude maps of the signal for the harmonics relating to the frequencies of 3, 7 and 11 Hz are reported in Figure 6.

By increasing the loading frequency, the contrast between the damaged area and the healthy one is reduced, suggesting that the defect is not superficial but sub-superficial. This evaluation is purely qualitative; a quantitative evaluation can only be carried out after a calibration.

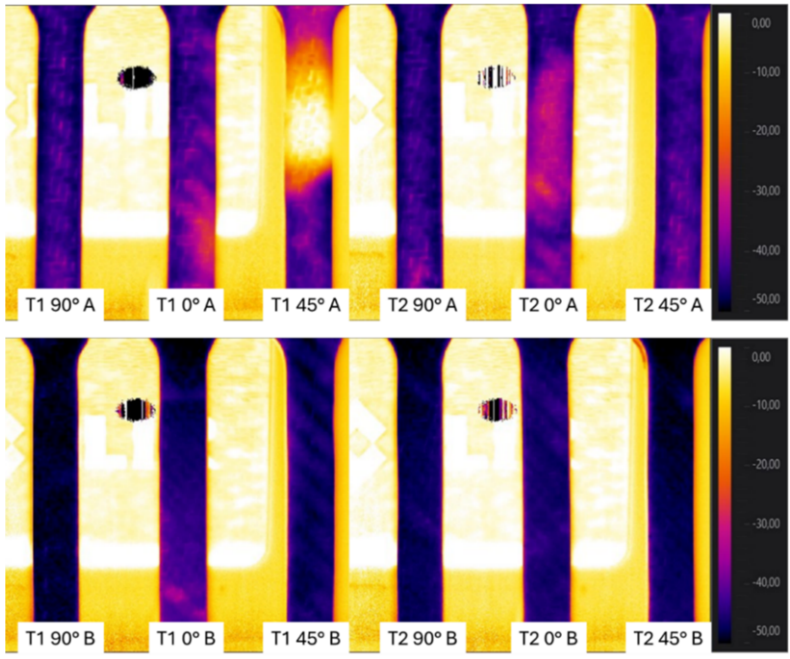


**Figure 4.** LT phase maps for the tensile samples for a heating period of 5s

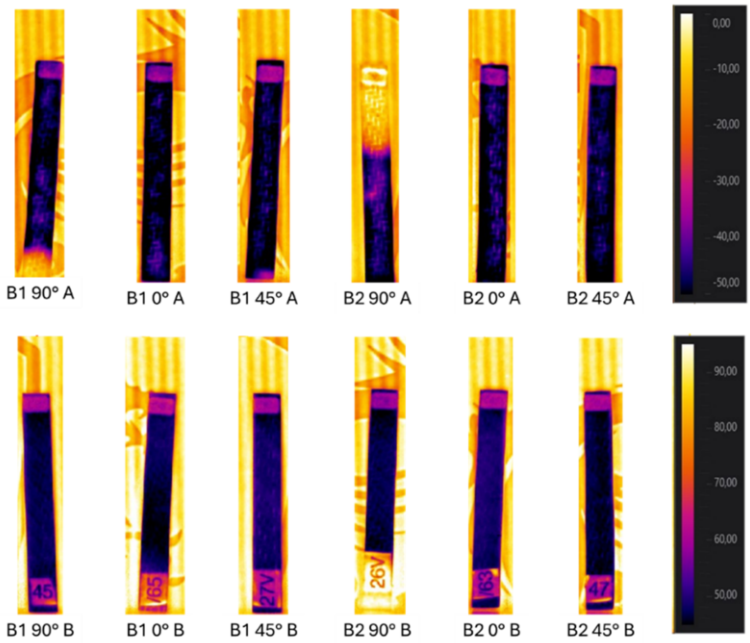


**Figure 5.** LT phase maps for the bending test samples for a heating period of 5s

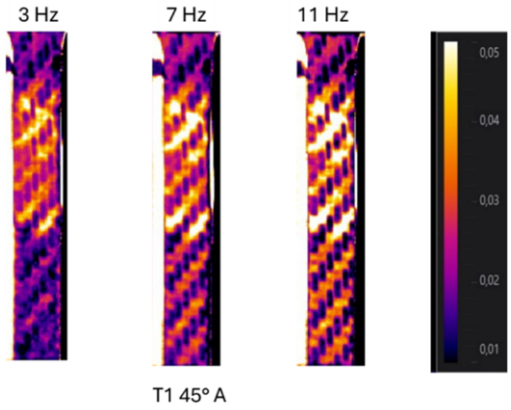


**Figure 6.** TSA phase maps for the bending samples for excitation frequencies of 3, 7 and 11 Hz

### *5.3. Tensile tests*

The stress-strain curves recorded for the six dog-bone specimens subjected to tensile tests are shown in Figure 7. Stress was calculated by dividing the load (in N), as measured by the load cell, by the specimen's effective cross-sectional area. Strain, in turn, was determined by dividing the change in displacement by the initial gauge length of the useful section.

All specimens showed similar behavior, including a first stretch of linear elastic deformation and a second stretch of plastic deformation followed by abrupt stress variations determined by the breaking of the fibers up to the breaking of the aluminum core. Young's modulus was determined by calculating the slope of the initial, linear portion of the curve.

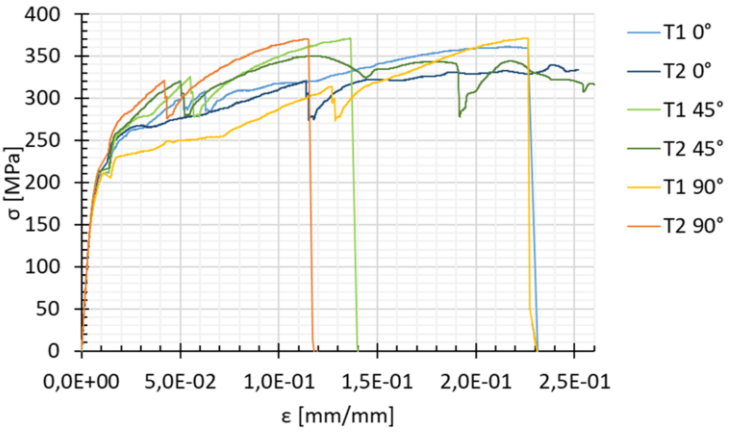


**Figure 7.** stress-strain curves recorded for the six dog-bone specimens subjected to tensile tests

Table 1 presents the mechanical characteristics obtained from the stress-strain curves.

The following mechanical characterization quantities were evaluated: the modulus of elasticity (E), the maximum stress reached before the coating fails ($\sigma_{max}$), the breaking stress of the aluminum core ($\sigma_u$).

A comparison of these values with the results from thermographic inspections suggests that delamination in the T1 45° specimen could be responsible for its lower Young's modulus compared to the others. However, due to high data variability and the small number of available defective specimens, this correlation cannot be statistically validated.

**Table 1.** Mechanical characteristics resulting from tensile tests for dog bone specimens

| Sample | E [GPa] | $\sigma_{max}$ [MPa] | $\sigma_u$ [MPa] |
|---|---|---|---|
| T1 0° | 62,60 | 208,14 | 359,55 |
| T2 0° | 61,23 | 210,41 | 333,06 |
| T1 45° | 60,05 | 208,92 | 370,51 |
| T2 45° | 62,03 | 212,90 | 317,05 |
| T1 90° | 64,71 | 210,55 | 371,10 |
| T2 90° | 69,04 | 213,78 | 369,80 |

### *5.4. Bending tests*

The bending test results are presented in terms of force-displacement curves (Figure 8), and the mechanical characteristics evaluated are the load at the first fracture of the coating fibers ($F_{max}$) and the load at the fracture of the aluminum core ($F_u$). Indeed, similarly to the tension tests, it was always possible to observe an initial linear elastic

deformation phase followed by a plastic deformation phase in which several fiber fractures occurred, causing sudden reductions in the load value.

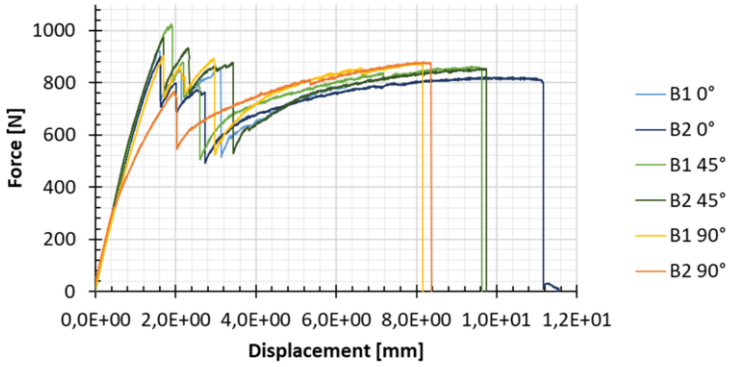


**Figure 8.** Force-Displacement curves recorded for the six rectangular specimens subjected to bending tests

**Table 2.** Mechanical characteristics resulting from bending tests for rectangular specimens

| Sample | $F_{max}$ [N] | $F_u$ [N] |
|---|---|---|
| B1 0° | 930,84 | 785,8 |
| B2 0° | 899,76 | 791,94 |
| B1 45° | 1024,22 | 845,87 |
| B2 45° | 973,88 | 844,17 |
| B1 90° | 903,26 | 861,48 |
| B2 90° | 767,38 | 871,27 |

Comparing the mechanical test results (Table 2) with those from the thermographic tests (Figure 5), a correlation between the presence of defects and reduced mechanical performance is again evident. Specifically, sample B2 90°, which was the only component where debonding was detected in the most highly stressed region during testing, exhibited a lower load at the first fiber fracture ($F_{max}$). Notably, it was also the only sample where this load was below the ultimate fracture load ($F_u$).

## 6. Conclusions

In this study, mechanical test specimens for tensile and bending testing, consisting of an AM aluminum alloy core bonded with carbon fiber laminates, were analyzed using thermographic NDTs to identify potential bonding defects.

Lock-in Thermography and TSA tests were shown to be capable of qualitatively detecting debonding in the specimens.

The subsequent mechanical characterization tests also allowed a correlation between inadequate layer adhesion and mechanical performance.

The reduced number of defective specimens, however, prevented the statistical validation of the conclusions reached in these tests. Therefore, this work serves as a preliminary study that needs to be validated with a more extensive experimental campaign.

## Acknowledgment

This study shows the results of the research activities of the Research Project PRIN PNRR 2022 “LODE” (circuLar economy-Oriented DEsign using hybrid-dissimilar joints and sustainable materials for lightweight structures), project funded by the Italian Ministry of Scientific and Technological Research

## References

[1] 29. Kharghani, N.; Guedes Soares, C. Experimental and numerical study of hybrid steel-FRP balcony overhang of ships under shear and bending. Mar. Struct. 2018, 60, 15–33.
[2] Palomba G, Corigliano P, Crupi V, Epasto G. and Guglielmino E, Static and Fatigue Full-Scale Tests on a Lightweight Ship Balcony Overhang with Al/Fe Structural Transition Joints, J. Mar. Sci. Eng. 2022, 10, 1382. https://doi.org/10.3390/jmse10101382
[3] Ayob, F. Joining of Dissimilar Materials by Diffusion Bonding/ Diffusion Welding for Ship Application. Marine Frontier. 2010; 1(2): 69-73.
[4] Findik, F. Recent developments in explosive welding. Material Design 2011; 32(3): 1081-1093, doi: 10.1016/j.matdes.2010.10.017
[5] Rashkovets, M., Dell’Avvocato, G., Contuzzi, N. et al. On the role of rotational speed in P-FSSW dissimilar aluminum alloys lap weld. Weld World (2025). https://doi.org/10.1007/s40194-025-02010-9.
[6] Dell’Avvocato G, Palumbo D, (2024), Thermographic procedure for the assessment of Resistance Projection Welds (RPW): Investigating parameters and mechanical performances, Journal of Advanced Joining Processes, 9, 100177, doi: 10.1016/j.jajp.2023.100177.
[7] Dell’Avvocato G, Bison P, Palmieri ME, Ferrarini G, Palumbo D, Tricarico L. Galietti U, (2024), Non-destructive estimation of mechanical properties in Usibor® 1500 via thermal diffusivity measurements: A thermographic procedure, NDT and E International, 143, 103034, doi: 10.1016/j.ndteint.2023.103034.
[8] Maldague XP V. Nondestructive Evaluation of Materials by Infrared Thermography. London: Springer London; 1993. https://doi.org/10.1007/978-1-4471-1995-1.
[9] Breitenstein O, Warta W, Langenkamp M. Lock-in Thermography. vol. 10. Berlin, Heidelberg: Springer Berlin Heidelberg; 2010. https://doi.org/10.1007/978-3-642-02417-7.
[10] Almond DP, Pickering SG. An analytical study of the pulsed thermography defect detection limit. J Appl Phys 2012;111. https://doi.org/10.1063/1.4704684.
[11] Chatterjee K, Tuli S, Pickering SG, Almond DP. A comparison of the pulsed, lock-in and frequency modulated thermography nondestructive evaluation techniques. NDT and E International 2011;44:655–67. https://doi.org/10.1016/j.ndteint.2011.06.008.
[12] Pickering S, Almond D. Matched excitation energy comparison of the pulse and lock-in thermography NDE techniques. NDT and E International 2008;41:501–9. https://doi.org/10.1016/j.ndteint.2008.05.007.
[13] Almond DP, Angioni SL, Pickering SG. Long pulse excitation thermographic non-destructive evaluation. NDT and E International 2017;87:7–14. https://doi.org/10.1016/j.ndteint.2017.01.003.
[14] Dulieu-Barton JM, Stanley P (1998) Development and applications of thermoelastic stress analysis. J. Strain Analysis 33: 93-104
[15] Pitarresi G, Patterson EA (1999) A review of the general theory of thermoelastic stress analysis. J. Strain Analysis 35:35-39.
[16] Harwood N, Cummings WM (1991) Thermoelastic Stress Analysis, National Engineering Laboratory, Adam Hilger, Bristol, Philadelphia, New York.
[17] Di Carolo F, De Finis R, Palumbo D, Galietti U, (2019), A thermoelastic stress analysis general model: Study of the influence of biaxial residual stress on aluminium and titanium. Metals, 9(6), 671.